

# Reciprocal theorems for calculating the flow rate of oscillatory channel flows

Shrihari D. Pande,<sup>1,\*</sup> Evgeniy Boyko,<sup>2,\*</sup> and Ivan C. Christov<sup>1,†</sup>

<sup>1</sup>*School of Mechanical Engineering, Purdue University, West Lafayette, Indiana 47907, USA*

<sup>2</sup>*Faculty of Mechanical Engineering, Technion – Israel Institute of Technology, Haifa 3200003, Israel*

(Dated: December 19, 2023)

We demonstrate the use of the Lorentz reciprocal theorem in obtaining corrections to the flow rate for oscillatory flow in channels. We start from the unsteady Stokes equations and derive the suitable reciprocity relations for both rigid and deformable channels, assuming all quantities can be expressed as time-harmonic phasors. For the case of a rigid channel, the auxiliary problem is a steady flow solution, and the reciprocal theorem allows us to calculate the first-order correction in the Womersley number to the steady flow rate. For the case of a deformable channel, we account for the fluid–structure interaction using domain perturbation under the assumption of a small compliance number. Using the oscillatory flow solution in a rigid channel as the auxiliary problem, we obtain the first-order correction in the compliance number to the rigid channel flow rate. This correction, validated against numerical simulations, provides the leading-order effect of the interplay between the oscillations of the fluid flow and the compliance of the channel for arbitrary values of the Womersley number.

## 1. INTRODUCTION

Low-Reynolds-number oscillatory flows are widely encountered in microfluidics applications such as the generation of emulsions, mixing of fluids, and particle or cell separation [1]. Traditionally, the channels in these applications [1–4] are considered rigid, and it is of interest to determine the hydraulic impedance [5] (i.e., the complex hydrodynamic resistance [6]) due to the oscillatory flow. In recent years, new applications have emerged harnessing oscillatory flows through deformable channels. For example, lab-on-a-chip technologies use compliant components to achieve frequency conversion and flow control [7–9]. Meanwhile, in biofluid mechanics applications, compliant channels are used to mimic the physiology of human organs [10, 11], through which air or blood is cycled periodically [12–14]. These oscillations can be imposed [15] onto the compliant conduits, as in peristalsis [16], or they can be self-induced [17–19].

Accurate modeling and design of such compliant systems require a quantitative understanding of the relationship between key integrated quantities, such as flow rate and pressure drop, due to oscillatory flow. One approach to obtaining such relations is to solve the “complete” elasto-hydrodynamic problem, meaning to solve the coupled governing unsteady equations of elasticity and fluid flow [20]. Since the flow causes deformation, and the deformation of the conduit affects the flow, these equations are *two-way coupled*, giving rise to nonlinear moving-boundary problems that are difficult to solve either analytically or numerically [21]. To overcome this challenge, domain perturbation [22, 23] can be used to decouple the governing equations for small departures from the initial uniform conduit shape. However, even with this simplification, there is still the need to solve unsteady partial differential equations (PDEs) whose analytical solutions are unwieldy [24, 25]. An alternative approach, within the lubrication approximation, is to introduce the pressure-dependent channel deformation into the unidirectional oscillatory flow solution, which yields a complex-valued nonlinear PDE for the pressure [26]. To make further analytical progress, a small parameter must be introduced, such as the parameter quantifying the coupling between flow and deformation. Often, the oscillation frequency can also be assumed to be small compared to the viscous time scale (i.e., the Womersley number is small) [27, 28].

Another useful approach for finding the flow rate and pressure drop is to exploit the Lorentz reciprocal theorem [29], which allows the calculation of integrated quantities *without* the need for calculating the detailed velocity and pressure fields (see, e.g., [30, 31] and the references therein). This approach is particularly well-suited for low-Reynolds-number fluid mechanics applications such as those described above. For example, the reciprocal theorem has been used to predict the forces on and velocities of particles in oscillating flow fields [32–37], as well as the lift force on particles in steady motion near elastic walls (see, e.g., [38, 39] and the references therein). Although many applications of the reciprocal theorem are to three-dimensional flows, two-dimensional external oscillatory flows caused by the motion of immersed surfaces can also be handled [40, 41]. Furthermore, when combined with the lubrication approximation for slender flow geometries [42], the reciprocal theorem has also been used to obtain closed-form analytical expressions for

---

\* These authors contributed equally.

† Email address for correspondence: [christov@purdue.edu](mailto:christov@purdue.edu)

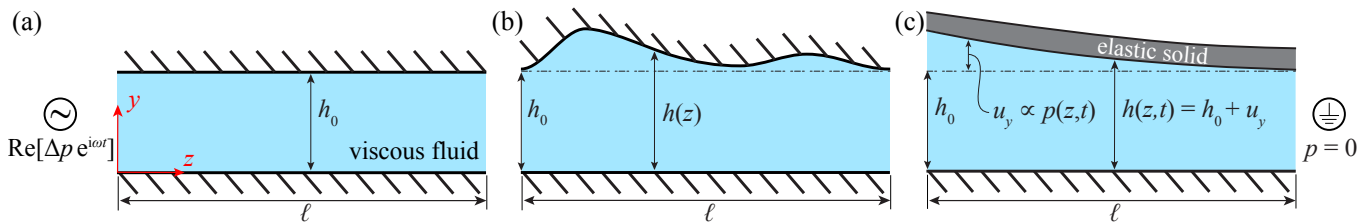


FIG. 1: Schematic illustration of the three planar geometries considered: (a) a straight rigid channel, (b) a nonuniform rigid channel, and (c) a deformable channel. The rigid channel has a height  $h_0$ , which is also the inlet/outlet height of the nonuniform channel and the undeformed height of the deformable channel. The channel axial length is  $\ell \gg h_0$ . An oscillatory viscous fluid flow is driven by an imposed pressure difference,  $\text{Re}[\Delta p e^{i\omega t}]$ , with the outlet ( $z = \ell$ ) pressure setting the gage. We are interested in determining the resulting flow rate  $q$ . For a slender deformable channel, the displacement  $u_y$  of the elastic top wall is caused by the hydrodynamic pressure.

flow rate–pressure drop relations for steady non-Newtonian flows through rigid channels [43, 44] and steady Newtonian flows through deformable channels [44]. However, despite all the progress made, to the best of our knowledge, no application of the reciprocal theorem to *oscillatory channel flows* has been presented to date. This observation motivates our study, which aims to show the reciprocal theorem’s versatility and simplicity for studying the two-way coupling between oscillatory flow and channel deformation.

In this work, we study oscillatory flows in two-dimensional channels, as in section 2, and demonstrate how to use the Lorentz reciprocal theorem to determine the flow rate, eliminating the need for the detailed calculation of the velocity and pressure fields. First, in section 3, we consider low-Womersley-number Newtonian oscillatory flow through a straight rigid channel and, in section 4, through a nonuniform rigid channel. We formulate the reciprocal theorem under the lubrication approximation and use the known steady pressure-driven flow solution for straight and nonuniform rigid channels to obtain the leading-order correction in the Womersley number due to oscillations. Then, in section 5, we consider Newtonian oscillatory flow through a weakly deformable channel without restrictions on the value of the Womersley number. Specifically, we use the known oscillatory flow solution for a straight rigid channel, in conjunction with domain perturbation, to obtain the leading-order correction due to compliance in the deformable channel.

## 2. PROBLEM FORMULATION

We consider the oscillatory low-Reynolds-number flow of a Newtonian fluid in three configurations, as shown in figure 1. The first configuration is a straight rigid channel (figure 1(a)), the second is a nonuniform rigid channel with a spatially varying top wall (figure 1(b)), and the third is a soft channel with a deformable top wall (figure 1(c)). We assume that the axial length of the channel,  $\ell$ , is much greater than the channel height  $h$ , i.e., we consider slender geometries. The viscous fluid flow is driven by an imposed oscillatory pressure difference with amplitude  $\Delta p$  and frequency  $\omega$ , resulting in a velocity field  $\mathbf{v}$  and a pressure distribution  $p$ . Our goal is to determine the flow rate  $q$ .

The governing equations for this type of fluid motion are those of unsteady Stokes flow [30, 45]:

$$\nabla \cdot \mathbf{v} = 0, \quad \nabla \cdot \boldsymbol{\sigma}_f = \rho_f \frac{\partial \mathbf{v}}{\partial t} \quad \text{with} \quad \boldsymbol{\sigma}_f = -p\mathbf{I} + 2\mu_f \mathbf{E}, \quad (2.1)$$

where  $\mathbf{I}$  is the identity tensor,  $\mathbf{E} = \frac{1}{2}[\nabla \mathbf{v} + (\nabla \mathbf{v})^\top]$  is the rate-of-strain tensor,  $\mu_f$  is the fluid’s dynamic viscosity, and  $\rho_f$  is the fluid’s density. For equations (2.1) to hold, the Reynolds number  $\text{Re} = \rho_f v_c h_0 / \mu_f$  must be small, where  $v_c$  is the characteristic axial velocity scale and  $h_0$  is either the rigid channel’s height, the inlet/outlet height of the nonuniform channel, or the undeformed height of the deformable channel. The governing equations for the displacement  $\mathbf{u}$  of the elastic top wall are not given, as we do not solve them in this work; instead, we use a simple model in section 5 below.

Specifically, we are only concerned with post-transient (“steady”) oscillations so that we can express the primary variables of the problem as *phasors*:

$$\mathbf{v} = \text{Re}[\mathbf{v}_a e^{i\omega t}], \quad p = \text{Re}[p_a e^{i\omega t}], \quad \boldsymbol{\sigma}_f = \text{Re}[\boldsymbol{\sigma}_{f,a} e^{i\omega t}], \quad \mathbf{u} = \text{Re}[\mathbf{u}_a e^{i\omega t}]. \quad (2.2)$$

where the quantities with an ‘a’ subscript are *amplitudes*. Using equation (2.2), and the linearity of the continuity and momentum equations (2.1), we obtain

$$\nabla \cdot \mathbf{v}_a = 0, \quad \nabla \cdot \boldsymbol{\sigma}_{f,a} = \rho_f \omega i \mathbf{v}_a \quad \text{with} \quad \boldsymbol{\sigma}_{f,a} = -p_a \mathbf{I} + 2\mu_f \mathbf{E}_a. \quad (2.3)$$

Next, we introduce the dimensionless variables,

$$T = \frac{t}{t_c}, \quad Y = \frac{y}{h_0}, \quad Z = \frac{z}{\ell}, \quad V_y = \frac{v_y}{\epsilon v_c}, \quad V_z = \frac{v_z}{v_c}, \quad P = \frac{p}{p_c}, \quad H = \frac{h}{h_0}, \quad U = \frac{u_y}{u_c}, \quad (2.4)$$

where  $p_c = \mu_f v_c \ell / h_0^2$  is the characteristic lubrication pressure scale,  $u_c$  is the characteristic scale of deformation (to be related to  $p_c$  via an elasticity model) of the top wall [46], and  $t_c = 1/\omega$  is the characteristic time scale.

We consider only planar geometries and analyze the problems per unit width. The flow is driven by an imposed pressure drop, which leads to  $p_c = \Delta p$  so that the characteristic axial velocity scale is  $v_c = h_0^2 \Delta p / (\mu_f \ell)$  and, consequently, the characteristic flow rate scale is  $q_c = h_0 v_c = h_0^3 \Delta p / (\mu_f \ell)$ . The regime of imposed flow rate is considered in the Appendix.

In addition, we introduce the Womersley number  $Wo = h_0 \sqrt{\rho_f \omega / \mu_f}$ , which represents the ratio of the square root of the viscous time scale,  $h_0^2 \rho_f / \mu_f$ , to the oscillatory time scale,  $\omega^{-1}$ , and the compliance number  $\beta = u_c / h_0$ , which can be reinterpreted to quantify the resistance to deformation of the top wall compared to the hydrodynamic pressure [46].

### 3. OSCILLATORY FLOW IN A STRAIGHT RIGID CHANNEL

Consider the straight rigid channel, shown in figure 1(a), such that  $H = 1$ .

#### (a). Exact solution for the flow rate–pressure drop relation

The flow in a straight channel is unidirectional such that  $\mathbf{V} = V_z(Y, T) \mathbf{e}_z$  [45]. Introducing the phasors (2.2) and the dimensionless variables (2.4), equations (2.3) reduce to

$$\frac{\partial^2 V_{z,a}}{\partial Y^2} - \frac{\partial P_a}{\partial Z} = Wo^2 i V_{z,a}, \quad \frac{\partial P_a}{\partial Y} = 0, \quad (3.1)$$

subject to no slip along the channel walls,  $V_{z,a}(Y = 0) = V_{z,a}(Y = 1) = 0$ . We are interested in the flow driven by a time-harmonic, oscillatory pressure distribution with the gage pressure fixed at  $Z = 1$ , thus:

$$-\frac{\partial P_a}{\partial Z} = \Delta P_a \quad \iff \quad P_a(Z) = \Delta P_a(1 - Z). \quad (3.2)$$

Now, it is straightforward to show that the solution to equations (3.1), taking into account (3.2), is

$$V_{z,a}(Y) = \frac{1}{iWo^2} \left[ 1 - \frac{\cos(i^{3/2}(1 - 2Y)Wo/2)}{\cos(i^{3/2}Wo/2)} \right] \Delta P_a. \quad (3.3)$$

This form of the solution and its  $Wo$  expansion is also given by Panton [47, section 11.7] (see also [48, §24] for a similar but not identical discussion). From equation (3.3), the dimensionless volumetric flow rate's amplitude is

$$Q_a = \int_0^1 V_{z,a}(Y) dY = f_0(Wo) \Delta P_a, \quad (3.4)$$

where for convenience, and later use, we have defined

$$f_0(Wo) \stackrel{\text{def}}{=} \frac{1}{iWo^2} \left[ 1 - \frac{1}{i^{3/2}Wo/2} \tan(i^{3/2}Wo/2) \right] \\ = \begin{cases} \frac{1}{12} - i\frac{1}{120}Wo^2 - \frac{17}{20160}Wo^4 + O(Wo^6), & Wo \ll 1, \\ 0 - i\frac{1}{Wo^2} + \dots, & Wo \gg 1. \end{cases} \quad (3.5)$$

Figure 2(a) shows the real and imaginary parts of the function  $f_0(Wo)$  given in equation (3.5), with black and red dashed curves representing the small- and large- $Wo$  asymptotic expressions (see also the related discussion in [2, 5]).

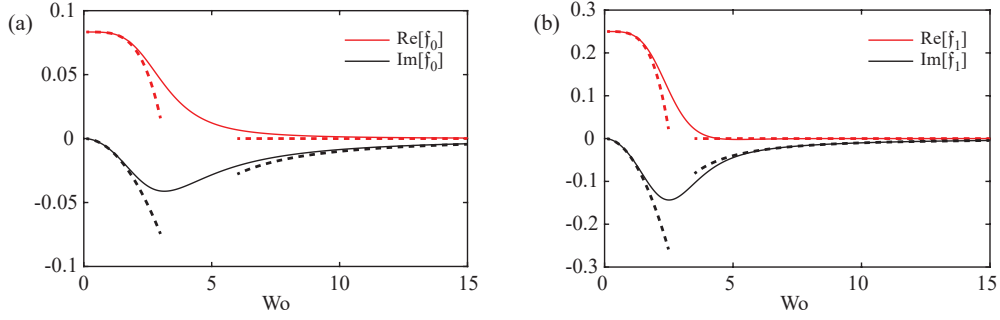


FIG. 2: The real and imaginary parts of the functions (a)  $f_0(\text{Wo})$  and (b)  $f_1(\text{Wo})$  from equations (3.5) and (5.11), respectively. Black and red dashed curves represent the small- and large- $\text{Wo}$  asymptotic expressions (given in the latter equations).

### (b). Reciprocal theorem for the flow rate–pressure drop relation

Let  $\hat{\mathbf{v}}$ ,  $\hat{p}$ , and  $\hat{\boldsymbol{\sigma}}_f$  denote, respectively, the velocity, pressure, and stress fields corresponding to the *steady* solution of the pressure-driven flow in a rigid two-dimensional channel, satisfying

$$\nabla \cdot \hat{\mathbf{v}} = 0, \quad \nabla \cdot \hat{\boldsymbol{\sigma}}_f = \mathbf{0} \quad \text{with} \quad \hat{\boldsymbol{\sigma}}_f = -\hat{p}\mathbf{I} + 2\mu_f \hat{\mathbf{E}}. \quad (3.6)$$

Forming the product of the momentum balances in equations (2.3) and (3.6), with  $\hat{\mathbf{v}}$  and  $\mathbf{v}_a$ , respectively, and using the usual vector identities, incompressibility, and the symmetry of the stress tensor [31, 44], we obtain

$$\nabla \cdot (\boldsymbol{\sigma}_{f,a} \cdot \hat{\mathbf{v}}) - \boldsymbol{\sigma}_{f,a} : \hat{\mathbf{E}} = \rho_f \omega i \mathbf{v}_a \cdot \hat{\mathbf{v}}, \quad (3.7a)$$

$$\nabla \cdot (\hat{\boldsymbol{\sigma}}_f \cdot \mathbf{v}_a) - \hat{\boldsymbol{\sigma}}_f : \mathbf{E}_a = 0. \quad (3.7b)$$

Subtracting these identities and using the stress tensors given in equations (2.3) and (3.6), yields

$$\nabla \cdot (\boldsymbol{\sigma}_{f,a} \cdot \hat{\mathbf{v}}) - \nabla \cdot (\hat{\boldsymbol{\sigma}}_f \cdot \mathbf{v}_a) = \rho_f \omega i \mathbf{v}_a \cdot \hat{\mathbf{v}}. \quad (3.8)$$

Finally, we integrate equation (3.8) over the entire fluid volume  $\mathcal{V}$  bounded by the surfaces of the top and bottom walls, and the surfaces at the inlet and outlet ( $S_0$  and  $S_\ell$  at  $z = 0$  and  $z = \ell$ , respectively). Then, applying the divergence theorem over the fluid domain  $\mathcal{V}$  leads to the reciprocal theorem in the form

$$\int_{S_0} \mathbf{n} \cdot \boldsymbol{\sigma}_{f,a} \cdot \hat{\mathbf{v}} \, dS + \int_{S_\ell} \mathbf{n} \cdot \boldsymbol{\sigma}_{f,a} \cdot \hat{\mathbf{v}} \, dS - \int_{S_0} \mathbf{n} \cdot \hat{\boldsymbol{\sigma}}_f \cdot \mathbf{v}_a \, dS - \int_{S_\ell} \mathbf{n} \cdot \hat{\boldsymbol{\sigma}}_f \cdot \mathbf{v}_a \, dS = \rho_f \omega i \int_{\mathcal{V}} \mathbf{v}_a \cdot \hat{\mathbf{v}} \, d\mathcal{V}, \quad (3.9)$$

similar to [37]. Here,  $\mathbf{n}$  is the unit outward normal to  $S_{0,\ell}$ . Note that the integrals over the bottom and top walls of the channel vanish because of the no-slip and no-penetration boundary conditions,  $\hat{\mathbf{v}}_a = \mathbf{v}_a = \mathbf{0}$ , there.

Using the dimensionless variables from equation (2.4) and performing a scaling analysis under the lubrication approximation (i.e., neglecting terms that are of  $\mathcal{O}(\epsilon^2)$ ) as in [43, 44], we obtain

$$\mathbf{n} \cdot \boldsymbol{\sigma}_{f,a} \cdot \hat{\mathbf{v}}|_{z=0,\ell} = \mp \frac{\mu_f v_c^2 \ell}{h_0^2} \left[ -P_a \hat{V}_z \right]_{Z=0,1}, \quad (3.10a)$$

$$\mathbf{n} \cdot \hat{\boldsymbol{\sigma}}_f \cdot \mathbf{v}_a|_{z=0,\ell} = \mp \frac{\mu_f v_c^2 \ell}{h_0^2} \left[ -\hat{P} V_{z,a} \right]_{Z=0,1}, \quad (3.10b)$$

where the minus sign in equations (3.10) corresponds to  $S_0$  and the plus sign corresponds to  $S_\ell$ .

Substituting equations (3.10) into equation (3.9), and using the outlet boundary condition  $P_a(Z = 1) = \hat{P}(Z = 1) = 0$ , we obtain

$$\int_0^1 \left[ P_a \hat{V}_z \right]_{Z=0} dY - \int_0^1 \left[ \hat{P} V_{z,a} \right]_{Z=0} dY = i \text{Wo}^2 \int_0^1 \int_0^1 V_{z,a} \hat{V}_z \, dY dZ. \quad (3.11)$$

Noting that  $P_a = P_a(Z)$ ,  $\hat{P} = \hat{P}(Z)$ ,  $\int_0^1 \hat{V}_z \, dY \stackrel{\text{def}}{=} \hat{Q}$ , and  $\int_0^1 V_{z,a} \, dY \stackrel{\text{def}}{=} Q_a$ , equation (3.11) yields the reciprocal theorem for the oscillatory flow of a Newtonian fluid in a two-dimensional channel:

$$\Delta P_a \hat{Q} = \Delta \hat{P} Q_a + i \text{Wo}^2 \int_0^1 \int_0^1 V_{z,a} \hat{V}_z \, dY dZ. \quad (3.12)$$

Equation (3.12) clearly shows that the dimensionless amplitude of the flow rate (or pressure drop) depends on the velocity amplitude  $V_{z,a}$ , and thus, generally, requires solving the complete oscillatory flow problem. However, in the weakly oscillatory limit, corresponding to  $\text{Wo}^2 \ll 1$ , we can apply the reciprocal theorem (3.12) to obtain the *leading-order oscillatory correction to the flow rate* using only the steady solution of the problem. To this end, we expand the amplitude of velocity into perturbation series in the dimensionless parameter  $\text{Wo}^2 \ll 1$ ,

$$V_{z,a} = \hat{V}_z + \text{Wo}^2 V_{z,a,1} + \text{O}(\text{Wo}^4), \quad (3.13)$$

where  $V_{z,a,1}$  is the first-order correction to the amplitude of the axial velocity due to the oscillatory pressure gradient. The remaining calculations are thus all accurate to  $\text{O}(\text{Wo}^2)$ . The dimensionless solution of the *steady* flow in a two-dimensional straight channel for a pressure-drop-controlled regime is

$$\hat{Q} = \frac{\Delta \hat{P}}{12}, \quad \hat{V}_z(Y) = \frac{1}{2} \Delta \hat{P} (1 - Y) Y. \quad (3.14)$$

Now, employing the expansion from equation (3.13) and substituting  $\hat{V}_z$  from equation (3.14) into equation (3.12), we have

$$\Delta P_a \hat{Q} = \Delta \hat{P} Q_a + i \text{Wo}^2 \int_0^1 \int_0^1 \hat{V}_z^2 dY dZ = \Delta \hat{P} Q_a + i \frac{1}{120} (\Delta \hat{P})^2 \text{Wo}^2. \quad (3.15)$$

Finally, substituting  $\hat{Q}$  from equation (3.14) and imposing  $\Delta P_a = \Delta \hat{P} = 1$  (consistent with our pressure-drop-controlled regime), we obtain

$$Q_a = \frac{1}{12} \left( 1 - i \frac{1}{10} \text{Wo}^2 \right), \quad (3.16)$$

which is in agreement with equation (3.4) using the  $\text{Wo} \ll 1$  expansion from equation (3.5).

#### 4. OSCILLATORY FLOW IN A NONUNIFORM RIGID CHANNEL

Now, consider a nonuniform channel with a *given* shape, as shown in figure 1(b), such that  $H(Z) \neq 1$ .

##### (a). Lubrication solution for the flow rate–pressure drop relation

To study the unsteady Stokes flow in a nonuniform channel, we consider further the limit of small channel aspect ratio  $\epsilon = h_0/\ell \ll 1$  such that the reduced Reynolds number  $\epsilon \text{Re} \ll 1$ . This limit is the well-known *lubrication approximation* [45]. This leads us again to equation (3.1) [26]. However, the pressure gradient cannot be constant in  $Z$ , thus equation (3.2) becomes

$$-\frac{\partial P_a}{\partial Z} = \Delta P_a \mathfrak{A}'(Z) \quad \iff \quad P_a(Z) = \Delta P_a \mathfrak{A}(Z), \quad (4.1)$$

where primes denote differentiation with respect to the argument. The amplitude definition in equation (4.1) requires the normalization  $\int_0^1 \mathfrak{A}'(Z) dZ = \mathfrak{A}(1) - \mathfrak{A}(0) = 1$ . In principle,  $\mathfrak{A}(Z)$  is determined from the given shape variation  $H(Z)$ .

As in section 3(a), it is straightforward to show that

$$V_{z,a}(Y, Z) = \frac{1}{i \text{Wo}^2} \left[ 1 - \frac{\cos(i^{3/2}(1-2Y)\text{Wo}H(Z)/2)}{\cos(i^{3/2}\text{Wo}H(Z)/2)} \right] \Delta P_a \mathfrak{A}'(Z). \quad (4.2)$$

From equation (4.2), the volumetric flow rate's amplitude is found to be

$$Q_a = \int_0^{H(Z)} V_{z,a}(Y, Z) dY = \frac{H(Z)}{i \text{Wo}^2} \left[ 1 - \frac{1}{i^{3/2}\text{Wo}H(Z)/2} \tan(i^{3/2}\text{Wo}H(Z)/2) \right] \Delta P_a \mathfrak{A}'(Z), \quad (4.3)$$

which must be constant since the cross-sectional area does not change in time. Then, for an imposed pressure drop, rearranging equation (4.3) and integrating from  $Z = 0$  to  $Z = 1$ , we obtain

$$Q_a \int_0^1 \frac{i \text{Wo}^2}{H(Z)} \left[ 1 - \frac{1}{i^{3/2}\text{Wo}H(Z)/2} \tan(i^{3/2}\text{Wo}H(Z)/2) \right]^{-1} dZ = \Delta P_a. \quad (4.4)$$

(b). **Reciprocal theorem for the flow rate–pressure drop relation**

For a nonuniform rigid channel, the reciprocal theorem can be derived in the same way as in section 3, leading to the following generalization of equation (3.11):

$$\int_0^{H(0)} [P_a \hat{V}_z]_{Z=0} dY - \int_0^{H(0)} [\hat{P} V_{z,a}]_{Z=0} dY = i\text{Wo}^2 \int_0^1 \int_0^{H(Z)} V_{z,a} \hat{V}_z dY dZ. \quad (4.5)$$

Noting that  $P_a = P_a(Z)$ ,  $\hat{P} = \hat{P}(Z)$ ,  $\int_0^{H(Z)} \hat{V}_z dY \stackrel{\text{def}}{=} \hat{Q}$ , and  $\int_0^{H(Z)} V_{z,a} dY \stackrel{\text{def}}{=} Q_a$ , yields the reciprocal theorem for oscillatory flow of a Newtonian fluid in a two-dimensional rigid but *nonuniform* channel:

$$\Delta P_a \hat{Q} = \Delta \hat{P} Q_a + i\text{Wo}^2 \int_0^1 \int_0^{H(Z)} V_{z,a} \hat{V}_z dY dZ, \quad (4.6)$$

where the dimensionless solution of the *steady* pressure-driven flow in a two-dimensional nonuniform channel for a pressure-drop-controlled regime is now

$$\hat{Q} = \frac{\Delta \hat{P}}{12 \int_0^1 H(Z)^{-3} dZ}, \quad \hat{V}_z(Y, Z) = \frac{\Delta \hat{P}}{2 \int_0^1 H(Z)^{-3} dZ} \left[ 1 - \frac{Y}{H(Z)} \right] \frac{Y}{H(Z)^2}. \quad (4.7)$$

Using the expansion (3.13) and  $\hat{V}_z$  from equation (4.7), equation (4.6) becomes

$$\begin{aligned} \Delta P_a \hat{Q} &= \Delta \hat{P} Q_a + i\text{Wo}^2 \int_0^1 \int_0^{H(Z)} \hat{V}_z^2 dY dZ \\ &= \Delta \hat{P} Q_a + i \frac{1}{120 \int_0^1 H(Z)^{-3} dZ} (\Delta \hat{P})^2 \text{Wo}^2 \int_0^1 \frac{1}{H(Z)} dZ. \end{aligned} \quad (4.8)$$

Finally, substituting  $\hat{Q}$  from equation (4.7) and imposing  $\Delta P_a = \Delta \hat{P} = 1$ , we obtain

$$Q_a = \frac{1}{12 \int_0^1 H(Z)^{-3} dZ} \left[ 1 - i \frac{1}{10} \text{Wo}^2 \int_0^1 \frac{1}{H(Z)} dZ \right], \quad (4.9)$$

which one could readily verify is in agreement with the small-Wo expansion of equation (4.4).

## 5. OSCILLATORY FLOW IN A DEFORMABLE CHANNEL

Now, consider a *deformable* channel, as shown in figure 1(c), with shape  $H(Z, T) = 1 + \beta U(Z, T)$ , for some displacement  $U$  of the top wall to be specified below.

(a). **Domain perturbation**

We proceed by the domain perturbation approach to this problem introduced by Boyko *et al.* [44]. Specifically, we expand the velocity, pressure, and stress fields' amplitudes into perturbation series in the compliance number  $\beta = u_c/h_0 \ll 1$ :

$$\mathbf{v}_a = \hat{\mathbf{v}}_a + \beta \mathbf{v}_{a,1} + \text{O}(\beta^2), \quad (5.1a)$$

$$p_a = \hat{p}_a + \beta p_{a,1} + \text{O}(\beta^2), \quad (5.1b)$$

where  $\mathbf{v}_{a,1}$  and  $p_{a,1}$  are the first-order corrections to the velocity and pressure's phasor amplitudes in the *rectangular domain* due to the deformation of the top wall. The remaining calculations are thus all accurate to  $\text{O}(\beta)$ . Note that, in the domain perturbation expansion, at each order of  $\beta$ , we necessarily solve a linear problem. Thus, it is appropriate to expand only the phasor amplitudes of the *primary variables* without including higher harmonics beyond  $e^{iT}$ . Likewise, we could also define, accordingly, expansions for the stress and rate of strain tensors, which are anyway determined by the velocity and pressure, as

$$\boldsymbol{\sigma}_{f,a} = \hat{\boldsymbol{\sigma}}_{f,a} + \beta \boldsymbol{\sigma}_{f,a,1} + \text{O}(\beta^2), \quad (5.1c)$$

$$\mathbf{E}_a = \hat{\mathbf{E}}_a + \beta \mathbf{E}_{a,1} + \text{O}(\beta^2). \quad (5.1d)$$

On the other hand,  $\hat{\mathbf{v}}_a$ ,  $\hat{p}_a$ , and  $\hat{\boldsymbol{\sigma}}_{f,a}$  denote, respectively, the phasor amplitudes of the velocity, pressure, and stress fields corresponding to the solution of the oscillatory pressure-driven flow in a *straight and rigid* two-dimensional channel (section 3 (a)), without restriction on the Womersley number.

**(b). Reciprocal theorem for the flow rate–pressure drop relation**

As discussed above,  $\mathbf{v}_a$ ,  $p_a$ , and  $\boldsymbol{\sigma}_{f,a}$  satisfy the phasor version of unsteady Stokes flow, namely equation (2.3), in the deformed channel. But,  $\hat{\mathbf{v}}_a$ ,  $\hat{p}_a$ , and  $\hat{\boldsymbol{\sigma}}_{f,a}$  also satisfy the unsteady Stokes flow equations, namely

$$\nabla \cdot \hat{\mathbf{v}}_a = 0, \quad \nabla \cdot \hat{\boldsymbol{\sigma}}_{f,a} = \rho_f \omega i \hat{\mathbf{v}}_a \quad \text{with} \quad \hat{\boldsymbol{\sigma}}_{f,a} = -\hat{p}_a \mathbf{I} + 2\mu_f \hat{\mathbf{E}}_a, \quad (5.2)$$

in the straight rigid channel. Substituting the perturbation expansion (5.1) into equation (2.3) and using equation (5.2), we obtain

$$\nabla \cdot \mathbf{v}_{a,1} = 0, \quad \nabla \cdot \boldsymbol{\sigma}_{f,a,1} = \rho_f \omega i \mathbf{v}_{a,1} \quad \text{with} \quad \boldsymbol{\sigma}_{f,a,1} = -p_{a,1} \mathbf{I} + 2\mu_f \mathbf{E}_{a,1}, \quad (5.3)$$

at  $O(\beta)$ . Forming the products of the momentum balances in equations (5.3) and (5.2), with  $\hat{\mathbf{v}}_a$  and  $\mathbf{v}_{a,1}$ , respectively, and using incompressibility, and the symmetry of the stress tensor, we obtain, as usual,

$$\nabla \cdot (\boldsymbol{\sigma}_{f,a,1} \cdot \hat{\mathbf{v}}_a) - \boldsymbol{\sigma}_{f,a,1} : \hat{\mathbf{E}}_a = \rho_f \omega i \mathbf{v}_{a,1} \cdot \hat{\mathbf{v}}_a, \quad (5.4a)$$

$$\nabla \cdot (\hat{\boldsymbol{\sigma}}_{f,a} \cdot \mathbf{v}_{a,1}) - \hat{\boldsymbol{\sigma}}_{f,a} : \mathbf{E}_{a,1} = \rho_f \omega i \hat{\mathbf{v}}_a \cdot \mathbf{v}_{a,1}. \quad (5.4b)$$

Subtracting these identities and using the stress tensors given in equations (5.3) and (5.2) yields

$$\nabla \cdot (\boldsymbol{\sigma}_{f,a,1} \cdot \hat{\mathbf{v}}_a) - \nabla \cdot (\hat{\boldsymbol{\sigma}}_{f,a} \cdot \mathbf{v}_{a,1}) = 0, \quad (5.5)$$

similar to [32]. Next, we integrate equation (5.5) over the entire fluid volume  $\mathcal{V}$  bounded by the surfaces of the top and bottom walls *in the undeformed state*, and the surfaces at the inlet and outlet ( $S_0$  and  $S_\ell$  at  $z = 0$  and  $z = \ell$ , respectively). Then, as shown in [44], applying the divergence theorem over the fluid domain  $\mathcal{V}$  leads to the reciprocal theorem in the form

$$\begin{aligned} \int_{S_0} \mathbf{n} \cdot \boldsymbol{\sigma}_{f,a,1} \cdot \hat{\mathbf{v}}_a \, dS + \int_{S_\ell} \mathbf{n} \cdot \boldsymbol{\sigma}_{f,a,1} \cdot \hat{\mathbf{v}}_a \, dS - \int_{S_0} \mathbf{n} \cdot \hat{\boldsymbol{\sigma}}_{f,a} \cdot \mathbf{v}_{a,1} \, dS \\ - \int_{S_\ell} \mathbf{n} \cdot \hat{\boldsymbol{\sigma}}_{f,a} \cdot \mathbf{v}_{a,1} \, dS - \int_{S_{\text{top}}} \mathbf{n} \cdot \hat{\boldsymbol{\sigma}}_{f,a} \cdot \mathbf{v}_{a,1} \, dS = 0. \end{aligned} \quad (5.6)$$

Note that the integrals over the bottom and top walls of the channel vanish because of the no-slip condition,  $\hat{\mathbf{v}}_a = \mathbf{v}_a = \mathbf{0}$ , there.

Using the dimensionless variables from equation (2.4) and performing a scaling analysis under the lubrication approximation (i.e., neglecting terms that are of  $O(\epsilon^2)$ ) as in [43, 44], we obtain

$$\mathbf{n} \cdot \boldsymbol{\sigma}_{f,a,1} \cdot \hat{\mathbf{v}}_a|_{z=0,\ell} = \mp \frac{\mu_f v_c^2 \ell}{h_0^2} \left[ -P_{a,1} \hat{V}_{z,a} \right]_{Z=0,1}, \quad (5.7a)$$

$$\mathbf{n} \cdot \hat{\boldsymbol{\sigma}}_{f,a} \cdot \mathbf{v}_{a,1}|_{z=0,\ell} = \mp \frac{\mu_f v_c^2 \ell}{h_0^2} \left[ -\hat{P}_a V_{z,a,1} \right]_{Z=0,1}. \quad (5.7b)$$

Substituting equations (5.7) into equation (5.6), and using the outlet boundary condition  $P_{a,1}(Z=1) = \hat{P}_a(Z=1) = 0$ , we obtain

$$\int_0^1 \Delta P_{a,1} \hat{V}_{z,a} \, dY - \int_0^1 \Delta \hat{P}_a V_{z,a,1} \, dY = \int_0^1 \left[ \frac{\partial \hat{V}_{z,a}}{\partial Y} V_{z,a,1} \right]_{Y=1} \, dZ. \quad (5.8)$$

Taking into account the domain-perturbation expansion (5.1) and the no-slip boundary condition  $V_{z,a}|_{Y=H(Z,T)} = 0$ , we have  $V_{z,a,1}|_{Y=1} = -U(Z,T)(\partial \hat{V}_{z,a} / \partial Y)|_{Y=1}$  as in [44], so that equation (5.8) becomes

$$\Delta P_{a,1} \hat{Q}_a - \Delta \hat{P}_a Q_{a,1} = - \int_0^1 U(Z,T) \left( \frac{\partial \hat{V}_{z,a}}{\partial Y} \Big|_{Y=1} \right)^2 \, dZ, \quad (5.9)$$

where we formally introduced  $\int_0^1 \hat{V}_{z,a} dY \stackrel{\text{def}}{=} \hat{Q}_a$  and  $\int_0^1 V_{z,a,1} dY \stackrel{\text{def}}{=} Q_{a,1}$  as before.

Recalling that  $U(Z, T) = \text{Re}[U_a e^{iT}]$  and  $\hat{V}_{z,a}(Y)$  is given by equation (3.3), equation (5.9) yields

$$\Delta P_{a,1} \hat{Q}_a - \Delta \hat{P}_a Q_{a,1} = -f_1(\text{Wo})(\Delta \hat{P}_a)^2 \int_0^1 \text{Re}[U_a e^{iT}] dZ, \quad (5.10)$$

where we have defined (see also [26])

$$f_1(\text{Wo}) \stackrel{\text{def}}{=} -\frac{1}{i\text{Wo}^2} \tan^2(i^{3/2}\text{Wo}/2) = \begin{cases} \frac{1}{4} - \frac{1}{24}\text{Wo}^2 i - \frac{17}{2880}\text{Wo}^4 + O(\text{Wo}^6), & \text{Wo} \ll 1, \\ 0 - \frac{1}{\text{Wo}^2} i + \dots, & \text{Wo} \gg 1. \end{cases} \quad (5.11)$$

Figure 2(b) shows the real and imaginary parts of the function  $f_1(\text{Wo})$  given in equation (5.11), with black and red dashed curves representing the small- and large-Wo asymptotic expressions.

To proceed with the calculation of the flow rate–pressure drop relation from equation (5.10), we must specify an elasticity model for  $U_a$ . For example, a Winkler-foundation-like mechanism [49–51] dictates that the local deformation is proportional to the local hydrodynamic pressure. Note that in this context, the Winkler-like foundation is understood to represent a width-averaged deformation of a 3D channel, as discussed in [19]; otherwise, inconsistencies arise [52] for incompressible 2D elastic solids (such as those considered in [50]). In dimensionless form, the Winkler-foundation-like mechanism yields  $U_a = P_a = \hat{P}_a + \beta P_{a,1} + O(\beta^2)$ . Further,  $\hat{P}_a(Z) = \Delta \hat{P}_a(1 - Z)$  with  $\Delta \hat{P}_a = 1$  and  $\Delta P_{a,1} = 0$  for a pressure-drop-controlled regime. Then, equation (5.10), at the lowest order in  $\beta$ , gives

$$Q_{a,1} = \frac{1}{2} \text{Re}[e^{iT}] f_1(\text{Wo}). \quad (5.12)$$

The nonlinear coupling caused by the fluid–structure interaction leads equation (5.12) to feature the phasor amplitude  $Q_{a,1}$  in addition to  $\text{Re}[e^{iT}]$ .

To understand the meaning of the result in equation (5.12), we interpret  $Q_{a,1}$  as the phasor amplitude of a first-order-in- $\beta$  correction  $Q_1$  to the flow rate, per the formal definition. Then,

$$Q_1 = \text{Re}[Q_{a,1} e^{iT}] = \text{Re} \left[ \frac{1}{2} \text{Re}[e^{iT}] f_1(\text{Wo}) e^{iT} \right] = \frac{1}{2} \text{Re} [f_1(\text{Wo}) e^{iT}] \text{Re}[e^{iT}]. \quad (5.13)$$

The last expression requires us to “endow meaning” to products of real parts. To this end, we note the identity [53, p. 188]:

$$\text{Re}[\mathbf{w}_1] \text{Re}[\mathbf{w}_2] = \frac{1}{2} \{ \text{Re}[\mathbf{w}_1 \mathbf{w}_2] + \text{Re}[\mathbf{w}_1 \mathbf{w}_2^*] \}, \quad (5.14)$$

for two complex numbers  $\mathbf{w}_1$  and  $\mathbf{w}_2$ , which is readily shown from the definition  $\text{Re}[\mathbf{w}] \stackrel{\text{def}}{=} (\mathbf{w} + \mathbf{w}^*)/2$ , where a ‘\*’ superscript denotes the complex conjugate. Then, employing the identity (5.14) and rearranging, equation (5.13) becomes

$$Q_1 = \frac{1}{4} \text{Re} [f_1(\text{Wo})(e^{2iT} + 1)], \quad (5.15)$$

which agrees as the leading-order-in- $\beta$  result from [26] obtained by a different method.

From equation (5.15), we can calculate the cycle-averaged flow rate as

$$\langle Q \rangle \stackrel{\text{def}}{=} \frac{1}{2\pi} \int_0^{2\pi} Q(T) dT = \langle \hat{Q} + \beta Q_1 \rangle + O(\beta^2) = \frac{\beta}{4} \text{Re}[f_1(\text{Wo})] + O(\beta^2), \quad (5.16)$$

having used the facts that  $\langle \hat{Q} \rangle = \langle \text{Re}[\hat{Q}_a e^{iT}] \rangle = 0$  and  $\langle \text{Re}[f_1(\text{Wo}) e^{2iT}] \rangle = 0$ . We note that equation (5.16) is identical to equation (24) in [26] obtained by a different method.

### (c). Illustrated example

In this subsection, we compare the flow rate expressions obtained using the reciprocal theorem to the reduced-order model introduced by Pande *et al.* [26], which is nonperturbative in  $\beta$ . Note that the model in Pande *et al.* [26] also



accounts for the nonlinear pressure evolution in the oscillatory flow state, which is quantified by a Strouhal number  $St = \ell/(t_c v_c)$ . The governing equation for the pressure evolution from [26] is

$$\frac{\partial}{\partial Z} \left\{ \left( \frac{1 + \beta \text{Re}[P]}{i\text{Wo}^2} \right) \left[ 1 - \frac{\tan(i^{3/2}\text{Wo}(1 + \beta \text{Re}[P])/2)}{i^{3/2}\text{Wo}(1 + \beta \text{Re}[P])/2} \right] \left( -\frac{\partial P}{\partial Z} \right) \right\} + \beta St \frac{\partial P}{\partial T} = 0. \quad (5.17)$$

The PDE (5.17) is solved numerically as described in [26] to obtain  $P(Z, T)$ , from which the flow rate  $Q(Z, T)$  is post-processed as the expression inside  $\{\dots\}$  in equation (5.17). The total inlet flow rate is then found by evaluating  $Q(Z, T)$  and  $Z = 0$ . Here, we are interested in the limit of  $St \rightarrow 0$ , so we use  $St = 10^{-4}$  for the simulation, having verified that making this value smaller in the simulation does not appreciably change the results. Below, we show the total inlet flow rate  $Q(Z = 0, T)$ , denoted simply as  $Q$ .

Figure 3 shows (a) the total flow rate  $Q$  and (b) the flow rate enhancement  $Q_1$  due to the channel compliance, as a function of  $T$  and for  $\text{Wo} = 1, 3, 5$  and  $\beta = 0.1$ . With respect to the model from [26],  $Q_1$  is obtained by subtracting the rigid-channel total flow rate,  $\hat{Q}$  found via equation (3.4), from the numerical solution for  $Q$  found via the PDE (5.17), and dividing by  $\beta$  (since  $Q = \hat{Q} + \beta Q_1$ ). We also show the low-Womersley approximations of  $Q$  and  $Q_1$ , based on the expansions (3.5) and (5.11), as dashed curves, for  $\text{Wo} = 1$ . We observe good agreement between the numerical solutions of the nonperturbative PDE and the results obtained using the reciprocal theorem for all values of Womersley numbers, with a maximum error of 10%.

From figure 3(a), we can also observe the well-known effect that a phase difference, which depends on the Womersley number, exists between the driving pressure drop,  $\propto \text{Re}[e^{iT}]$ , and the flow rate [54]. In this plot, the leading-order rigid-channel contribution dominates, and the phase is determined by  $f_0(\text{Wo})$  in equation (3.4). Moreover, we can also easily understand the phase difference from equation (3.16), wherein the first correction is  $i\text{Wo}^2$  (a  $90^\circ$  phase at that order). In figure 3(b), we observe that there is also a similar phase difference, increasing with the Womersley number, in the correction to the flow rate due to the channel's compliance. Now, the phase difference is determined by  $f_1(\text{Wo})$  in equation (5.15), from which we also observe that the frequency doubles, similar to the result for an oscillating particle near an elastic surface [35].

Another effect of the interplay of wall compliance and pressure oscillation is the time-independent term in equation (5.15), which leads to a nonzero cycle-averaged flow rate (5.16). To better understand this effect, in figure 4, we show (a) the cycle-averaged flow rate  $\langle Q \rangle$  and (b) the normalized cycle-averaged flow rate  $\langle Q \rangle/\beta$ , as functions of  $\text{Wo}$ , for different values of the compliance number  $\beta$ . It is evident that the value of cycle averaged flow rate is not zero, suggesting a presence of streaming flow [15, 26, 28]. Again, we observe that the numerical solution of the nonperturbative PDE is in good agreement with the theoretical prediction obtained using the reciprocal theorem. We also observe that the predicted normalized cycle average flow rate  $\langle Q \rangle/\beta$  is a universal function of  $\text{Wo}$ , as shown in figure 4(b). Additionally, the cycle-averaged flow rate  $\langle Q \rangle$  decreases with  $\text{Wo}$ , asymptotically approaching zero. This observation suggests the streaming is weaker at higher oscillation frequencies. This effect can be understood from equation (5.9), in which we see that the flow-induced deformation  $U$  and the squared wall shear stress  $(\partial \hat{V}_{z,a}/\partial Y)^2 \propto f_1(\text{Wo})$  are coupled. For large Womersley numbers, however, there is no flow across the bulk of the channel, and the velocity oscillations are confined to infinitesimally thin Stokes (boundary) layers near the walls. As  $\text{Wo} \rightarrow \infty$ , these layers

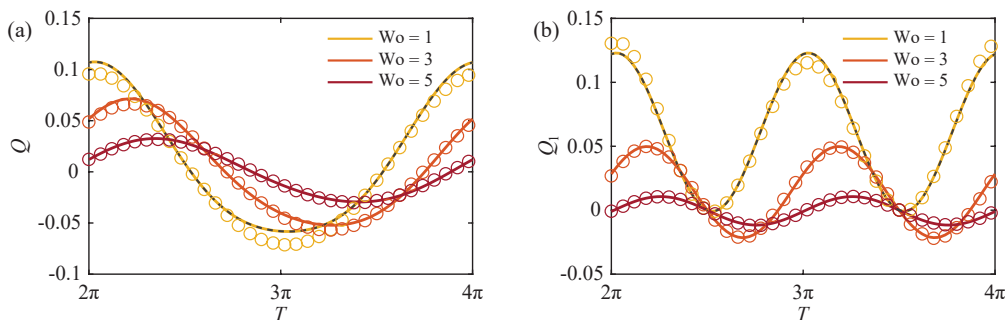


FIG. 3: Time evolution of the oscillatory flow rate in a deformable channel in the pressure-drop-controlled regime ( $\Delta \hat{P}_a = 1$ ). (a) The evolution of the flow rate  $Q$  as a function of dimensionless time  $T$ , for  $\text{Wo} = 1, 3, 5$  and  $\beta = 0.1$ . (b) The evolution of the flow rate enhancement  $Q_1$  as a function of  $T$  for  $\text{Wo} = 1, 3, 5$  and  $\beta = 0.1$ . Solid curves represent the results of the reciprocal theorem,  $Q = \text{Re}[(\hat{Q}_a + \beta Q_{a,1})e^{iT}]$ , where  $\hat{Q}_a = f_0(\text{Wo})\Delta \hat{P}_a$  is given by equation (3.4) and  $Q_{a,1}$  is given by equation (5.12). Black dashed curves represent the small- $\text{Wo}$  expansion using equations (3.5) and (5.11); note these overlap with the  $\text{Wo} = 1$  curves. Circles represent the results of the numerical solution of the nonperturbative PDE (5.17), which is not restricted to  $\beta \ll 1$ .

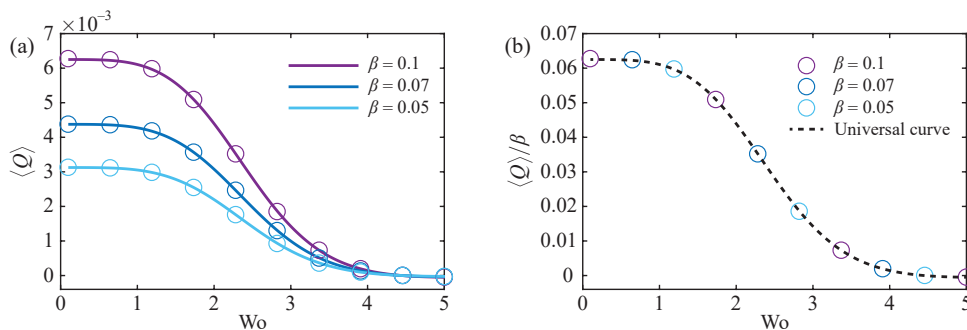


FIG. 4: (a) The streaming flow rate  $\langle Q \rangle$  as a function of the Womersley number  $Wo$  for different values of  $\beta$  obtained from equation (5.16) (solid curves) and the numerical solution of the nonperturbative PDE (5.17) (circles). (b) The universal profile  $\langle Q \rangle / \beta$  as a function of the Womersley number  $Wo$ , showing the collapse of the data and curves from (a) onto a single dashed curve,  $\frac{1}{4} \text{Re}[f_1(Wo)]$ , consistent with the theory.

vanish, leading to no velocity variations and no shear stresses anywhere across the channel. Indeed, in figure 2(b), we observe that  $f_1(Wo) \rightarrow 0$  rapidly with increasing  $Wo$ , and  $\langle Q \rangle \propto \text{Re}[f_1(Wo)]$  (see equation (5.16)).

## 6. CONCLUSION

In this work, using the Lorentz reciprocal theorem, we derived closed-form expressions for flow rates in rigid and deformable channels conveying oscillatory flows of Newtonian fluids. For the case of the rigid channel, we used the steady (Poiseuille) flow solution as the auxiliary problem to obtain the oscillatory flow rate up to  $O(Wo^2)$ . For the deformable channel, we used the rigid-channel oscillatory (Womersley) flow solution as the auxiliary problem to obtain the flow rate up to  $O(\beta)$  for arbitrary values of the Womersley number,  $Wo$ . Both the solutions obtained via the reciprocal theory were verified by comparing to the full Womersley solution for the rigid channel and to the reduced model proposed by [26] for the deformable channel in the appropriate limit ( $Wo \ll 1$  for rigid channel and  $\beta \ll 1$  for deformable channel), respectively. We observed good agreement for both of the solutions, thus validating our approach to finding analytical corrections to the flow rates of the well-known (auxiliary) problems.

Importantly, in the present approach, we bypassed solving the momentum equation (for the rigid channel) or the coupled elastohydrodynamic problem (for the deformable channel) in obtaining the leading-order effect of flow oscillations. As discussed in, e.g., [25, 26], solving the elastohydrodynamic for the oscillatory flow is particularly challenging. Our results show the simplicity and elegance of using the reciprocal theorem to efficiently obtain integrated quantities in multiphysics problems.

In future work, the presented approach can be applied to other oscillatory flows in compliant conduits. For example, an interesting extension of the present work, which considered only two-dimensional channels, is to calculate the first-order-in- $\beta$  flow rate correction in narrow axisymmetric tubes and three-dimensional channels of an initially rectangular cross-section. Indeed, since the oscillatory pressure-driven flow field for these rigid geometries is also known (see, e.g., [5] and the references therein), one can find the leading-order effect of the interplay between the flow oscillations, the channel wall's compliance, and the cross-sectional aspect ratio of the channel, on the flow rate. Furthermore, as a future research direction, it would be of particular interest to explore how the rheological response of complex fluids, such as shear thinning and viscoelasticity, affects the oscillatory flow rate in deformable channels.

## ACKNOWLEDGMENTS

*Data accessibility* MATLAB scripts required to run and analyze the numerical simulations of equation (5.17), and resulting data files are available on the Purdue University Research Repository [55]. All remaining results in this work are analytical and did not generate new data.

*Funding* E.B. gratefully acknowledges support from the Israel Science Foundation (Grant No. 1942/23). S.D.P. and I.C.C. acknowledge partial support from the U.S. National Science Foundation (Grant No. CMMI-2029540) during the completion of this work.

## APPENDIX. FLOW-RATE-CONTROLLED REGIMES

For a flow-rate-controlled regime, we impose  $q_c = q$ ; consequently,  $v_c = q/h_0$  and  $p_c = \mu_f q \ell / h_0^3$ .

### (a). Straight rigid channel

For a flow-rate-controlled regime, the dimensionless solution of the *steady* pressure-driven flow in a two-dimensional straight channel is

$$\Delta \hat{P} = 12 \hat{Q}, \quad \hat{V}_z(Y) = 6 \hat{Q} (1 - Y) Y, \quad (\text{A.1})$$

from which the calculation from section 3 (b) can be redone.

In this regime, imposing  $Q_a = \hat{Q} = 1$  and substituting equation (A.1) into equation (3.12) and using equation (3.13), we obtain

$$\Delta P_a = 12 + i \frac{6}{5} \text{Wo}^2 + \text{O}(\text{Wo}^4), \quad (\text{A.2})$$

which is in agreement with the small-Wo expansion of  $1/f_0(\text{Wo})$  from equation (3.4).

### (b). Nonuniform rigid channel

For the flow-rate-controlled regime, the dimensionless solution of the *steady* pressure-driven flow in a two-dimensional nonuniform rigid channel (see, e.g., [56]) is

$$\Delta \hat{P} = \int_0^1 \frac{12 \hat{Q}}{H(Z)^3} dZ, \quad \hat{V}_z(Y, Z) = 6 \hat{Q} \left[ 1 - \frac{Y}{H(Z)} \right] \frac{Y}{H(Z)^2}, \quad (\text{A.3})$$

from which the calculation from section 4 (b) can be redone.

In this regime, imposing  $Q_a = \hat{Q} = 1$  and substituting equation (A.3) into equation (4.6) and using equation (3.13), we obtain

$$\Delta P_a = 12 \int_0^1 \frac{dZ}{H(Z)^3} + i \frac{6}{5} \text{Wo}^2 \int_0^1 \frac{dZ}{H(Z)} + \text{O}(\text{Wo}^4), \quad (\text{A.4})$$

which is in agreement with small-Wo expansion of the left-hand side of equation (4.4).

### (c). Weakly deformable channel

For a flow-rate-controlled regime, the dimensionless solution of the oscillatory pressure-driven flow in a two-dimensional *straight and rigid* channel is

$$\Delta \hat{P}_a = \frac{\hat{Q}_a}{f_0(\text{Wo})}, \quad \hat{V}_{z,a}(Y) = \frac{1}{i \text{Wo}^2} \left[ 1 - \frac{\cos(i^{3/2}(1-2Y)\text{Wo}/2)}{\cos(i^{3/2}\text{Wo}/2)} \right] \frac{\hat{Q}_a}{f_0(\text{Wo})}, \quad (\text{A.5})$$

from which the calculation from section 5 (b) can be redone.

In this regime,  $Q_a = \hat{Q}_a = 1$  and  $Q_{a,1} = 0$ . Substituting equation (A.5) into equation (5.9) and recalling that  $U(Z, T) = \text{Re}[P_a e^{iT}] = \text{Re}[\hat{P}_a e^{iT}] + \text{O}(\beta)$  and  $\hat{P}_a(Z) = \frac{1}{f_0(\text{Wo})}(1 - Z)$ , we obtain

$$\Delta P_{a,1} = -\frac{f_1(\text{Wo})}{f_0(\text{Wo})^2} \int_0^1 \text{Re}[\hat{P}_a e^{iT}] dZ = -\frac{1}{2} \frac{f_1(\text{Wo})}{f_0(\text{Wo})^2} \text{Re} \left[ \frac{1}{f_0(\text{Wo})} e^{iT} \right]. \quad (\text{A.6})$$

To understand equation (A.6), we note that

$$\Delta P_1 = \text{Re}[\Delta P_{a,1} e^{iT}] = -\frac{1}{2} \text{Re} \left[ \frac{f_1(\text{Wo})}{f_0(\text{Wo})^2} \text{Re} \left[ \frac{1}{f_0(\text{Wo})} e^{iT} \right] e^{iT} \right]. \quad (\text{A.7})$$

Using the identity (5.14), equation (A.7) becomes

$$\Delta P_1 = -\frac{1}{4} \operatorname{Re} \left[ \frac{f_1(\text{Wo})}{f_0(\text{Wo})^3} e^{2iT} + \frac{f_1(\text{Wo})}{f_0(\text{Wo})|f_0(\text{Wo})|^2} \right]. \quad (\text{A.8})$$

Thus,

$$\langle \Delta P \rangle = \langle \Delta \hat{P} + \beta \Delta P_1 \rangle + O(\beta^2) = -\frac{\beta}{4} \operatorname{Re} \left[ \frac{f_1(\text{Wo})}{f_0(\text{Wo})|f_0(\text{Wo})|^2} \right] + O(\beta^2). \quad (\text{A.9})$$

- 
- [1] B. Dincau, E. Dressaire, and A. Sauret, Pulsatile flow in microfluidic systems, *Small* **16**, 1904032 (2020).
- [2] S. Vedel, L. H. Olesen, and H. Bruus, Pulsatile microfluidics as an analytical tool for determining the dynamic characteristics of microfluidic systems, *J. Micromech. Microeng.* **20**, 035026 (2010).
- [3] G. Vishwanathan and G. Juarez, Generation and application of sub-kilohertz oscillatory flows in microchannels, *Microfluid. Nanofluid.* **24**, 69 (2020).
- [4] S. M. Recktenwald, C. Wagner, and T. John, Optimizing pressure-driven pulsatile flows in microfluidic devices, *Lab Chip* **21**, 2605 (2021).
- [5] C. J. Morris and F. K. Forster, Oscillatory flow in microchannels, *Exp. Fluids* **36**, 928 (2004).
- [6] B. J. Kirby, *Micro- and Nanoscale Fluid Mechanics: Transport in Microfluidic Devices* (Cambridge University Press, New York, 2010).
- [7] D. C. Leslie, C. J. Easley, E. Seker, J. M. Karlinsey, M. Utz, M. R. Begley, and J. P. Landers, Frequency-specific flow control in microfluidic circuits with passive elastomeric features, *Nat. Phys.* **5**, 231 (2009).
- [8] M. R. Begley, M. Utz, D. C. Leslie, H. Haj-Hariri, J. Landers, and H. Bart-Smith, Periodic response of fluidic networks with passive deformable features, *Appl. Phys. Lett.* **95**, 203501 (2009).
- [9] M. D. Biviano, M. V. Paludan, A. H. Christensen, E. V. Østergaard, and K. H. Jensen, Smoothing oscillatory peristaltic pump flow with bioinspired passive components, *Phys. Rev. Appl.* **18**, 064013 (2022).
- [10] D. Huh, B. D. Matthews, A. Mammoto, M. Montoya-Zavala, H. Y. Hsin, and D. E. Ingber, Reconstituting organ-level lung functions on a chip, *Science* **328**, 1662 (2010).
- [11] S. N. Bhatia and D. E. Ingber, Microfluidic organs-on-chips, *Nat. Biotechnol.* **32**, 760 (2014).
- [12] C. A. Dragon and J. B. Grotberg, Oscillatory flow and mass transport in a flexible tube, *J. Fluid Mech.* **231**, 135 (1991).
- [13] J. B. Grotberg and O. E. Jensen, Biofluid mechanics in flexible tubes, *Annu. Rev. Fluid Mech.* **36**, 121 (2004).
- [14] M. Kiran Raj, S. Dasgupta, and S. Chakraborty, Biomimetic pulsatile flows through flexible microfluidic conduits, *Biomicrofluidics* **13**, 014103 (2019).
- [15] T. Parthasarathy, Y. Bhosale, and M. Gazzola, Elastic solid dynamics in a coupled oscillatory Couette flow system, *J. Fluid Mech.* **946**, A15 (2022), arXiv:2011.09453.
- [16] D. Takagi and N. J. Balmforth, Peristaltic pumping of viscous fluid in an elastic tube, *J. Fluid Mech.* **672**, 196 (2011).
- [17] M. Heil and A. L. Hazel, Fluid-structure interaction in internal physiological flows, *Annu. Rev. Fluid Mech.* **43**, 141 (2011).
- [18] T. J. Pedley and D. Pihler-Puzović, Flow and oscillations in collapsible tubes: Physiological applications and low-dimensional models, *Sādhāna: J. Indian Acad. Sci.* **40**, 891 (2015).
- [19] X. Wang and I. C. Christov, Reduced modelling and global instability of finite-Reynolds-number flow in compliant rectangular channels, *J. Fluid Mech.* **950**, A26 (2022).
- [20] Y. Bazilevs, K. Takizawa, and T. E. Tezduyar, *Computational Fluid-Structure Interaction Methods and Applications* (John Wiley & Sons Inc., Chichester, UK, 2013).
- [21] S. Čanić, Moving boundary problems, *Bull. Amer. Math. Soc.* **58**, 79 (2020).
- [22] M. D. Van Dyke, *Perturbation Methods in Fluid Mechanics* (Parabolic Press, 1975).
- [23] N. R. Lebovitz, Perturbation expansions on perturbed domains, *SIAM Rev.* **24**, 381 (1982).
- [24] S. Čanić, D. Lamponi, A. Mikelić, and J. Tambača, Self-consistent effective equations modeling blood flow in medium-to-large compliant arteries, *Multiscale Model. Simul.* **3**, 559 (2005).
- [25] S. Čanić, J. Tambača, G. Guidoboni, A. Mikelić, C. J. Hartley, and D. Rosenstrauch, Modeling viscoelastic behavior of arterial walls and their interaction with pulsatile blood flow, *SIAM J. Appl. Math.* **67**, 164 (2006).
- [26] S. D. Pande, X. Wang, and I. C. Christov, Oscillatory flows in compliant conduits at arbitrary Womersley number, *Phys. Rev. Fluids*, to appear, preprint (2023), arXiv:2304.00543.
- [27] S. B. Elbaz and A. D. Gat, Dynamics of viscous liquid within a closed elastic cylinder subject to external forces with application to soft robotics, *J. Fluid Mech.* **758**, 221 (2014).
- [28] V. Anand and I. C. Christov, Transient compressible flow in a compliant viscoelastic tube, *Phys. Fluids* **32**, 112014 (2020).
- [29] H. A. Lorentz, A general theorem concerning the motion of a viscous fluid and a few consequences derived from it (in Dutch), *Versl. Konigl. Akad. Wetensch. Amst.* **5**, 168 (1896).
- [30] J. Happel and H. Brenner, *Low Reynolds Number Hydrodynamics* (Martinus Nijhoff Publishers, The Hague, 1983).
- [31] H. Masoud and H. A. Stone, The reciprocal theorem in fluid dynamics and transport phenomena, *J. Fluid Mech.* **879**, P1 (2019).

- [32] W. Zhang and H. A. Stone, Oscillatory motions of circular disks and nearly spherical particles in viscous flows, *J. Fluid Mech.* **367**, 329 (1998).
- [33] A. M. Leshansky and J. F. Brady, Force on a sphere via the generalized reciprocal theorem, *Phys. Fluids* **16**, 843 (2004).
- [34] J. F. Collis, D. Chakraborty, and J. E. Sader, Autonomous propulsion of nanorods trapped in an acoustic field, *J. Fluid Mech.* **825**, 29 (2017).
- [35] A. Kargar-Estahbanati and B. Rallabandi, Lift forces on three-dimensional elastic and viscoelastic lubricated contacts, *Phys. Rev. Fluids* **6**, 034003 (2021).
- [36] I. Fouxon, B. Y. Rubinstein, and A. M. Leshansky, Excess shear force exerted on an oscillating plate due to a nearby particle, *Phys. Rev. Fluids* **8**, 054104 (2023).
- [37] Z. Zhang, V. Bertin, M. H. Essink, H. Zhang, N. Fares, Z. Shen, T. Bickel, T. Salez, and A. Maali, Unsteady drag force on an immersed sphere oscillating near a wall, *J. Fluid Mech.* **977**, A21 (2023).
- [38] L. Bureau, G. Coupier, and T. Salez, Lift at low Reynolds number, *Eur. Phys. J. E* **46**, 111 (2023).
- [39] B. Rallabandi, Fluid-elastic interactions near contact at low Reynolds number, *Annu. Rev. Fluid Mech.* **56**, to appear (2024).
- [40] W. H. Lin, Hydrodynamic forces on multiple circular cylinders oscillating in a viscous incompressible fluid, *Z. angew. Math. Mech.* **67**, 487 (1987).
- [41] G. J. Elfring, A note on the reciprocal theorem for the swimming of simple bodies, *Phys. Fluids* **27**, 023101 (2015).
- [42] R. F. Day and H. A. Stone, Lubrication analysis and boundary integral simulations of a viscous micropump, *J. Fluid Mech.* **416**, 197 (2000).
- [43] E. Boyko and H. A. Stone, Reciprocal theorem for calculating the flow rate–pressure drop relation for complex fluids in narrow geometries, *Phys. Rev. Fluids* **6**, L081301 (2021).
- [44] E. Boyko, H. A. Stone, and I. C. Christov, Flow rate–pressure drop relation for deformable channels via fluidic and elastic reciprocal theorems, *Phys. Rev. Fluids* **7**, L092201 (2022).
- [45] L. G. Leal, *Advanced Transport Phenomena: Fluid Mechanics and Convective Transport Processes* (Cambridge University Press, 2007).
- [46] I. C. Christov, V. Cognet, T. C. Shidhore, and H. A. Stone, Flow rate–pressure drop relation for deformable shallow microfluidic channels, *J. Fluid Mech.* **814**, 267 (2018).
- [47] R. L. Panton, *Incompressible Flow*, 4th ed. (John Wiley & Sons, Hoboken, NJ, 2013).
- [48] L. D. Landau and E. M. Lifshitz, *Fluid Mechanics*, 2nd ed., Course of Theoretical Physics, Vol. 6 (Pergamon Press, Oxford, 1987).
- [49] D. Coyle, Forward roll coating with deformable rolls: A simple one-dimensional elastohydrodynamic model, *Chem. Eng. Sci.* **43**, 2673 (1988).
- [50] J. M. Skotheim and L. Mahadevan, Soft lubrication, *Phys. Rev. Lett.* **92**, 245509 (2004).
- [51] X. Yin and S. Kumar, Lubrication flow between a cavity and a flexible wall, *Phys. Fluids* **17**, 063101 (2005).
- [52] T. G. J. Chandler and D. Vella, Validity of Winkler’s mattress model for thin elastomeric layers: beyond Poisson’s ratio, *Proc. R. Soc. A* **476**, 20200551 (2020).
- [53] R. B. Bird, R. C. Armstrong, and O. Hassager, *Dynamics of Polymeric Liquids. Volume 1: Fluid Mechanics*, 2nd ed. (John Wiley and Sons, New York, 1987).
- [54] P. S. Ayyaswamy, Introduction to biofluid mechanics, in *Fluid Mechanics*, edited by P. K. Kundu, I. M. Cohen, and D. R. Dowling (Academic Press, an imprint of Elsevier Inc., San Diego, CA, 2016) 6th ed., Chap. 16, pp. e1–e73.
- [55] S. D. Pande, X. Wang, and I. C. Christov, *MATLAB scripts and SimVascular case files for “Oscillatory flows in compliant conduits at arbitrary Womersley number”*, Purdue University Research Repository (2023).
- [56] B. Tavakol, G. Froehlicher, D. P. Holmes, and H. A. Stone, Extended lubrication theory: improved estimates of flow in channels with variable geometry, *Proc. R. Soc. A* **473**, 20170234 (2017).